Partial volume and motion correction in cardiac PET: First results from an in vs ex vivo comparison using animal datasets

A. Turco, PhD,[a,c] O. Gheysens, MD, PhD,[a,b] J. Duchenne, MSc,[c] J. Nuyts, PhD,[a] F. Rega, MD, PhD,[c,d] J. U. Voigt, MD, PhD,[c,e] K. Vunckx, PhD,[a] and P. Claus, PhD[c]

[a] Department of Imaging and Pathology, Nuclear Medicine and Molecular imaging, Medical Imaging Research Center (MIRC), KU Leuven - University of Leuven, Leuven, Belgium
[b] Department of Nuclear Medicine, University Hospitals Leuven, Leuven, Belgium
[c] Department of Cardiovascular Sciences, Medical Imaging Research Center (MIRC), KU Leuven - University of Leuven, Leuven, Belgium
[d] Department of Cardiac Surgery, University Hospitals Leuven, Leuven, Belgium
[e] Department of Cardiovascular Diseases, University Hospitals Leuven, Leuven, Belgium

Received Jun 1, 2017; accepted Nov 7, 2018
doi:10.1007/s12350-018-01581-z

Background. **In a previous study on ex vivo, static cardiac datasets, we investigated the benefits of performing partial volume correction (PVC) in cardiac ^{18}F-Fluorodeoxyglucose(FDG) PET datasets. In the present study, we extend the analysis to in vivo cardiac datasets, with the aim of defining which reconstruction technique maximizes quantitative accuracy and, ultimately, makes PET a better diagnostic tool for cardiac pathologies.**

Methods. **In vivo sheep datasets were acquired and reconstructed with/without motion correction and using several reconstruction algorithms (with/without resolution modeling, with/without non-anatomical priors). Corresponding ex vivo scans of the excised sheep hearts were performed on a small-animal PET scanner (Siemens Focus 220, microPET) to provide high-resolution reference data unaffected by respiratory and cardiac motion. A comparison between the in vivo cardiac reconstructions and the corresponding ex vivo ground truth was performed.**

Results. **The use of an edge-preserving prior (Total Variation (TV) prior in this work) in combination with motion correction reduces the bias in absolute quantification when compared to the standard clinical reconstructions (− 0.83 vs − 3.74 SUV units), when the end-systolic gate is considered. At end-diastole, motion correction improves absolute quantification but the PVC with priors does not improve the similarity to the ground truth more than a regular iterative reconstruction with motion correction and without priors. Relative quantification was not influenced much by the chosen reconstruction algorithm.**

Conclusions. **The relative ranking of the algorithms suggests superiority of the PVC reconstructions with dual gating in terms of overall absolute quantification and noise properties. A well-tuned edge-preserving prior, such as TV, enhances the noise properties of the resulting images of the heart. The end-systolic gate yields the most accurate quantification of cardiac datasets. (J Nucl Cardiol 2019;26:2034–44.)**

Key Words: Cardiac PET • Motion correction • Partial volume correction • Quantification

Electronic supplementary material The online version of this article (https://doi.org/10.1007/s12350-018-01581-z) contains supplementary material, which is available to authorized users.

The authors of this article have provided a PowerPoint file, available for download at SpringerLink, which summarizes the contents of the paper and is free for re-use at meetings and presentations. Search for the article DOI on SpringerLink.com.

Reprint requests: P. Claus, PhD, Department of Cardiovascular Sciences, Medical Imaging Research Center (MIRC), KU Leuven - University of Leuven, 3000 Leuven, Belgium; *piet.claus@kuleuven.be*

1071-3581/$34.00

Abbreviations	
^{18}F-FDG	^{18}F-fluorodeoxyglucose
PET	Positron emission tomography
PVE	Partial volume effect
PVC	Partial volume correction
OSEM	Ordered subsets expectation maximization (reconstruction algorithm)
RR	Resolution recovery
MAP	Maximum a posteriori (reconstruction algorithm)
TV	Total variation (prior)
SUV	Standard uptake values
LV	Left ventricular

See related editorial, pp. 2045–2047

INTRODUCTION

The characterization of cardiac pathologies by means of positron emission tomography (PET) is progressively increasing.[1] In recent years, it has been hypothesized that hemodynamic or mechanical indicators of the cardiac workload collected from a patient (e.g., left-ventricular (LV) pressure and/or myocardial deformation) can be correlated to specific uptake patterns of ^{18}F-FDG.[2] If such correlation was proven, PET images could have the potential to offer, in a non-invasive fashion, parameters useful to improve the assessment of the progression and the severity of cardiac pathologies. Additionally, it could better predict the responsiveness of patients to the planned therapeutic program (e.g., cardiac resynchronization therapy).

Regional differences in myocardial ^{18}F-FDG uptake have been observed in the past.[3] However, a regionally inhomogeneous wall thickness in remodeled hearts might cause an apparently different uptake within the reconstructed heart images due to the limited spatial resolution of the PET system. In a recent study,[4] we investigated the necessity of partial volume correction (PVC) techniques during reconstruction of cardiac datasets in a simplified scenario where no motion affected the datasets. In that study, the partial volume correction performance of iterative image reconstruction with resolution modeling and edge-preserving priors was evaluated. We considered both priors based on anatomical side information (e.g., from computed tomography) and non-anatomical priors that favor piecewise smoothness (e.g., the total variation (TV) prior[5]). The use of such non-anatomical priors had shown to improve the absolute quantification of the LV myocardium of the available datasets, when compared to the state-of-the-art iterative reconstruction algorithms (with or without resolution recovery).

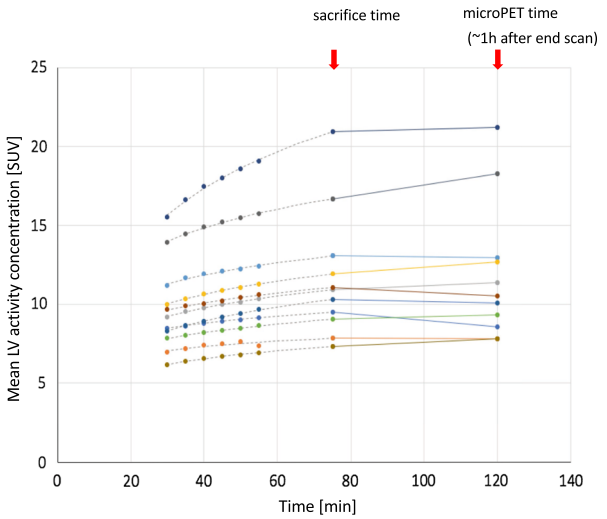

Figure 1. Mean LV activity concentration in Standard Uptake Values (SUV) for all sheep datasets (one animal per color). The first 6 time points represent the total LV wall activity in the polar maps of each dynamic reconstruction of the in vivo dataset. The activity at sacrifice is extrapolated based on the logarithmic trendline that fit the dynamic points. The last point is the total LV wall activity computed from the polar map of the ex vivo (microPET) dataset. All reconstructions have been corrected for decay to the beginning of the in vivo scan before the computation of the activities.

In addition, the motion of the heart during the entire PET examination—due to the heartbeat and to the breathing motion to which the heart is indirectly subject—causes additional uncertainty on the estimated tracer distribution. Several studies have highlighted the usefulness of motion correction techniques for the improved reconstruction of cardiac datasets.[6,7] However, the comparison of the obtained, motion-corrected datasets against a ground truth has not been performed yet. All previous studies perform a comparison between motion-corrected and static reconstructions, and report the improvements based on changes in specific indicators such as wall thickness, ejection fraction, or cavity volume.[8,9]

To our knowledge, the combination of motion correction and partial volume correction techniques for the reconstruction of cardiac datasets acquired on a clinical PET/CT scanner has not been thoroughly evaluated. The aim of this work is to utilize the available in and ex vivo animal datasets to investigate this issue.

METHODS

Thirteen Swifter x Charolais cross-breed female sheep with body weight 38 ± 3 kg were used for these experiments and subjected to the same pacing and imaging procedure. Each

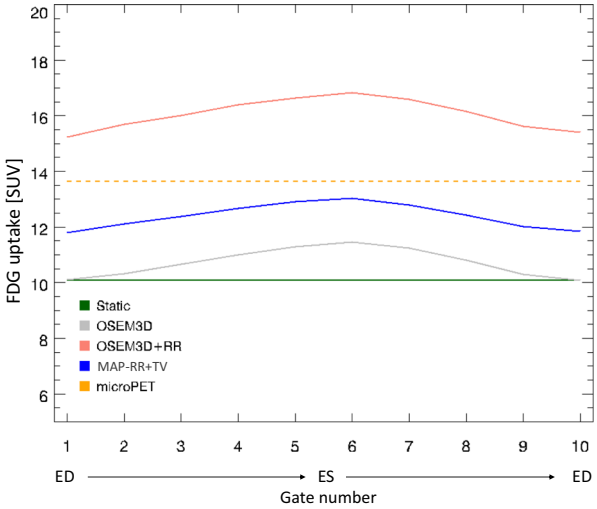

Figure 2. The max-count polar maps are computed for each sheep and for each cardiac gate at end-expiration, and the mean of all these polar maps is then calculated (similarly to the procedure in[4]) and plotted in this graph. The mean value over all sheep is reported for each gate and for each algorithm. The microPET was here downscaled with the statscale. The OSEM3D reconstruction was post-smoothed with a Gaussian kernel of 5 mm (FWHM).

animal had a pacemaker implanted, which was set to pace the heart at 180 beats per minute during 8 weeks to achieve dilated cardiomyopathy with asymmetric remodeling of the LV walls.[10] It was expected that different parts of such remodeled hearts would be affected differently by the partial volume effect (PVE) (e.g., the thinner septum was expected to be more affected by blurring, when compared to the lateral wall) and that therefore, PVC would have a significant effect on the tracer uptake analysis.

At 8 weeks, the remodeling of the heart reached a plateau and the imaging protocol was started. For all imaging procedures and measurements, the pacemaker of the sheep was set to a fixed heart rate of 110 beats/minute. The animals were anesthetized with isoflurane and mechanically ventilated with an endotracheal tube during all experimental procedures.

All procedures performed in this study involving animals were in accordance with the ethical standards of our institution (project number P146/2012) and complied with the European Commission Directive 2010/63/EU.

Acquisition of the Animal Datasets

Each of the animals went through euglycemic-hyperinsulinemic clamping to maximize glucose uptake in the heart.[11] Once steady-state was achieved, each sheep was injected with ^{18}F-FDG, and a PET scan of 30 minutes was performed (in vivo scan) 30 minutes post-injection on a clinical PET/CT scanner (Siemens Biograph 16, Hirez). The mean activity at the beginning of the in vivo scans was 310.5 (range 109-477) MBq. During this scan, the respiratory and cardiac motion of the animals were recorded with an Anzai AZ773V respiratory

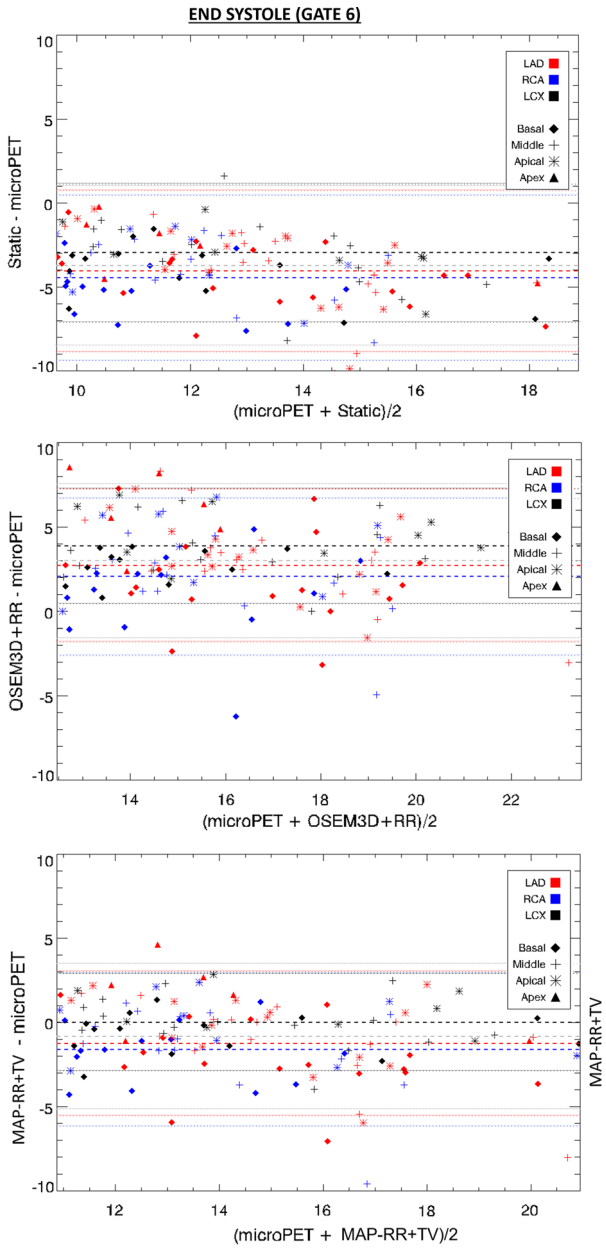

Figure 3. Bland-Altman (B-A) plots for the static (ungated), MAP − RR + TV (dual-gated), and OSEM3D + RR (dual-gated) reconstructions against the ground truth (microPET), at end-systole. Max-count polar maps were used to calculate the segmental values of both in and ex vivo datasets. The microPET was here scaled down using statscale. The segments are color-coded based on the vascular territory they belong to. (Red) *LAD*, left anterior descending artery segments; (blue) *RCA*, Right coronary artery segments; (black) *LCX*, left circumflex artery segments. Dashed lines indicate the bias, dotted lines indicate the limits of agreement. Gray lines represent the global trend.

belt and an ECG tracking device, to enable off-line motion correction of the in vivo datasets. An attenuation correction (AC) CT was acquired in a fixed cardiac and respiratory phase.

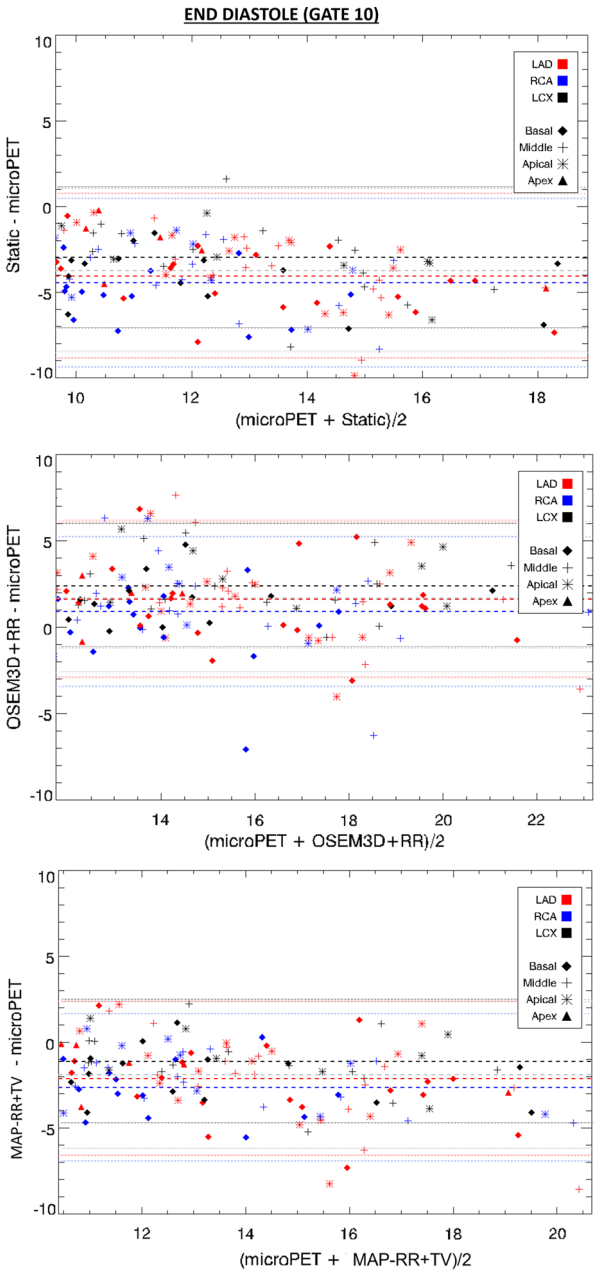

Figure 4. Bland-Altman (B-A) plots for the static (ungated), MAP − RR + TV (dual-gated), and OSEM3D + RR (dual-gated) reconstructions against the ground truth (microPET), at end-diastole.

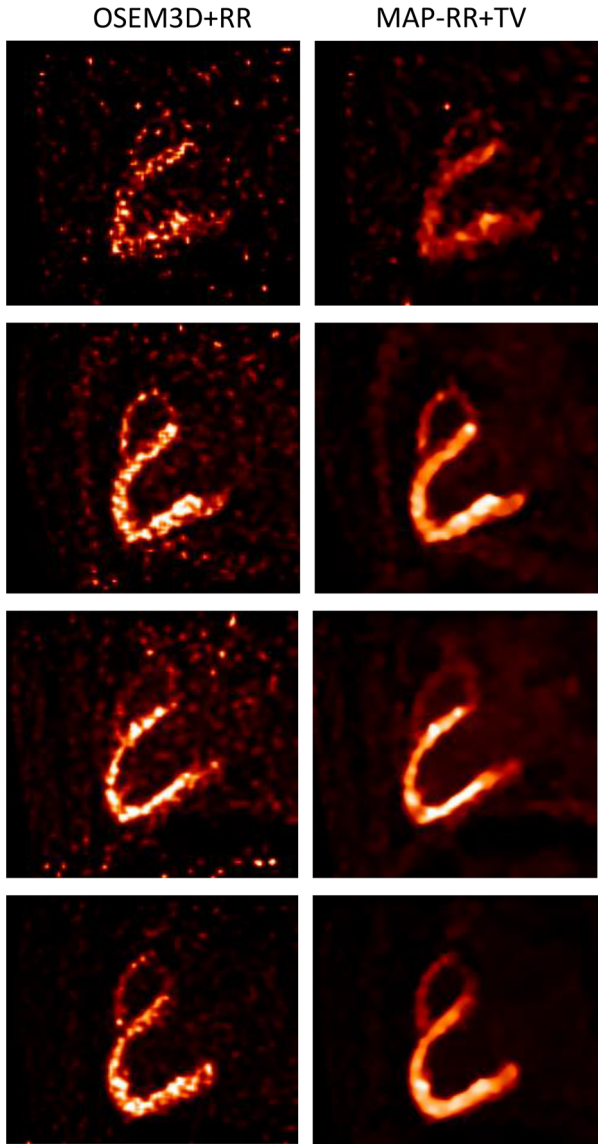

Figure 5. OSEM3D + RR (left) and MAP − RR + TV (right) reconstructions at end-systole. Five different animals with increasing count levels from top to bottom. The MAP − RR + TV reconstructions appear smoother and better defined.

This was achieved by disconnecting the endotracheal tube for the duration of the AC CT and by retrospectively gating the acquired CT for cardiac motion. Another AC CT was obtained in a fixed respiratory phase, using the same procedure as above, and no cardiac gating. After the scan, each sheep was sacrificed under isoflurane anesthesia with intravenous 160 mg/kg pentobarbital and 50 mL of saturated KCl. The mean time elapsed between the end of the in vivo scan and the sacrifice, calculated on 8 sheep datasets for which the approximate sacrifice time was available, was 21 minutes (min: 15/max: 32 minutes). The heart of each sheep was explanted immediately after sacrifice. Each heart was filled with a low-attenuating, hardening polyurethane foam. Once the foam was solid, a 15-minute PET scan on a small-animal PET scanner (Siemens Focus220 microPET) was performed, followed by a 10-minute transmission scan for scatter correction and a 20-minute PET scan of the same heart on the clinical PET/CT Hirez scanner. A high-dose, high-resolution (HR)CT was also acquired on the clinical PET/CT scanner for each of the ex vivo hearts. It was used both for attenuation correction (AC) and as anatomical information for both the microPET and the Hirez ex vivo datasets.

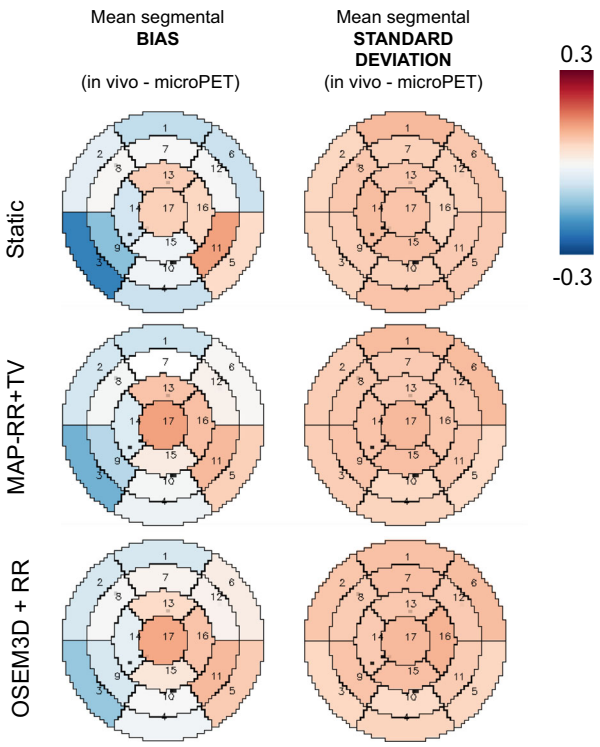

Figure 6. Polar plots displaying the mean bias and the mean standard deviation of the differences obtained by subtracting the normalized in vivo reconstructions (top pane: static, middle pane: MAP − RR + TV, bottom pane: OSEM3D + RR) from the normalized microPET polar maps. Average values over all animals.

Motion Correction of the In Vivo Datasets

The acquired in vivo animal PET datasets were either not corrected for motion (static datasets), or corrected for motion using a phase-based gating approach.[12] This approach was chosen to be consistent with the algorithm used by the scanner and was supported by the regularity of the breathing cycles. In the latter case, the initial dataset was split into 5 respiratory gates. The gate containing data corresponding to end-expiration was subsequently split into 10 cardiac gates. Each of the resulting gates contained the events collected in one particular cardiac and respiratory phase. Due to the very low amount of data resulting from the dual gating of the in vivo datasets, two of the sheep datasets could not be considered for the subsequent analysis.

Reconstruction of the Datasets

Ex vivo, ground-truth datasets. The purpose of this study was to compare the output of different correction methods to a ground-truth dataset, which was here represented by the ex vivo microPET datasets. Iterative reconstructions of the microPET images were performed as in[4](5 iterations × 28 subsets). These included resolution recovery and the application of an anatomy-based prior (asymmetrical Bowsher prior, w = 50, n = 9). A prior was applied because resolution recovery alone is known to reduce the apparent thickness of the structures and to possibly hamper quantification.[13] Moreover, Bowsher reconstructions have been shown to improve the recovery of activity concentrations.[14]

Static in vivo reconstructions. The **static** reconstructions were obtained using in-house developed software which attempted to reproduce as closely as possible a typical clinical reconstruction. 3D reconstructions using an iterative algorithm (ordered subsets expectation maximization, OSEM) were computed, using a ray-tracing projection without resolution modeling. The voxel size was set to 2.66 × 2.66 × 2 mm, and 4 iterations × 8 subsets were chosen.

Gated in vivo reconstructions. The algorithms that were used to reconstruct the dual-gated datasets were chosen based on our previous study on PVC of the ex vivo datasets[4]:

- a 3D OSEM reconstruction with resolution recovery (RR): OSEM + RR.
- an iterative reconstruction algorithm with prior information (maximum a posteriori, MAP) with RR: MAP − RR + TV. The prior information mitigates the artifacts produced by resolution modeling alone, and the noise that affects the reconstructions.[5] The MAP − RR + TV reconstructions were performed using a weight (β) of 0.005 for the prior, which defines its strength. This value was chosen based on a previous optimization study, where it proved to produce clinically acceptable images with improved noise properties.[15] Additionally, we verified that such choice yielded visually acceptable reconstructions also for the current datasets.

In-house developed software was used to perform the reconstruction of all the dual-gated datasets. A distance-driven projection method was used to ensure that all voxels are well sampled during the reconstruction.[16] These projectors are being recently integrated into clinical PET systems; thanks to their favorable numerical characteristics. A resolution recovery (RR) technique is however needed to account for the finite spatial resolution of the PET system. The RR was achieved by sinogram smoothing with a Gaussian function (full width at half-maximum (FWHM) =4.3/4.5 mm in the transaxial and axial directions, respectively).

In both the in vivo and ex vivo scans, the heart was positioned near the center of the field of view, where the resolution can be treated as shift-invariant with good approximation.[17] Hence, a spatially invariant resolution modeling approach was used as a best compromise between reconstruction time and image quality.

The voxel size of the reconstructed PET images was set to 1.35^3 mm^3. The iteration scheme consisted of 3i42s (i: iterations, s: subsets), followed by 2i24s and 2i1s.

Dynamic in vivo reconstructions. Our study analyzes ^{18}F-FDG PET reconstructions obtained from datasets acquired either 30 minutes post-injection (in vivo datasets) or

after the sacrifice of the animal (ex vivo datasets), which in turn occurred about 1.5 hours after tracer injection. Previous studies have documented a steady increase of FDG tracer uptake in the LV wall up to 3 hours after patient injection.[18]

Dynamic reconstructions of the available in vivo datasets were performed to verify whether the datasets used in this study were affected by such gradual increase of uptake. The original, ungated listmode was divided into 6 frames of equal length (5 minutes/frame). Each frame was individually reconstructed using a distance-driven projection method, resolution modeling in the sinogram space, the same iteration scheme as for the dual-gated reconstructions, and a voxel size of 2 mm in the three directions. Decay correction of each of the dynamic frames was performed to the beginning of the in vivo scan.

The breath-hold, cardiac-gated CT was used for the attenuation correction of all the aforementioned reconstructions. Scatter and randoms were also modeled during the reconstruction of these datasets, using the scatter and random estimates provided by third-party software (e7-tools, Siemens, Knoxville).

Image Post-processing: Polar Maps (or Bull's Eye Plots)

17-segments polar maps (PMs) or bull's eye plots of the LV wall were created according to the guidelines of the American Heart Association[19] to evaluate the relative and absolute activity distributions in comparison to the ground truth. The use of polar maps allowed to align the corresponding LV regions of the in vivo and ex vivo reconstructions without the need for a non-rigid registration between the two datasets. Additionally, polar maps are a commonly used tool to assess the tracer uptake in nuclear medicine studies.

Max-count polar maps. For each of the gated and static reconstructed datasets and for the ground truth, the bull's eye plots were created as described in.[20] The delineation of the LV wall was automatically performed by in-house software. Max-count polar maps were generated by taking the maximum value over the LV wall thickness at each radial and longitudinal position, within the automatically defined endocardial and epicardial contours. A fixed distance of 1.6 cm was imposed between the endocardial and the epicardial contours, to fully encompass the LV wall.

Mean-count polar maps, total activity, and scaling factor. Mean-count polar maps were generated for all datasets (gated, static, dynamic, ground truth) by taking the mean value over the LV wall thickness at each radial and longitudinal position, within the automatically defined endocardial and epicardial contours. A fixed distance of 1.6 cm was imposed between the endocardial and the epicardial contours, in order to fully encompass the LV wall while excluding as much as possible the influence of the left-ventricular blood pool and of the right ventricle from the computation of the total activity. Corresponding volumetric polar maps were also obtained, whose voxels indicate the volume of the corresponding section of the reconstruction. The multiplication and subsequent summation of all corresponding voxels of the mean-count polar maps and the volumetric polar maps generated the total LV wall activity for each of the reconstructions.

The total LV wall activity for each of the 6 dynamic frames was plotted against time, for each animal, together with the total LV wall activity computed from the ground-truth dataset. The total activity at sacrifice time (measurement not available) was obtained by applying a logarithmic fit to the LV wall activity values computed on the dynamic frames. Such logarithmic fit, which we expected would be representative of a biological process such as cardiac LV wall uptake, was performed to compare the sacrifice total LV wall activity value to the microPET value. This would thereby exclude any increases of activity between the sacrifice and the microPET scan. A paired t-test was performed between the extrapolated total activity at sacrifice time and the computed total activity on the microPET reconstructions, to test the efficacy of the logarithmic estimation.

Each curve in Figure 1 shows the activity of the dynamic reconstructions, the extrapolated activity at sacrifice time, and the microPET activity for a specific sheep. The logarithmic fit was optimal for all animals (mean $R^2 > 0.95$). The extrapolated sacrifice value matches well with the calculated total microPET activity (p-value of the paired t-test between the total extrapolated activity at sacrifice and the total microPET activity: $p = 0.24 > 0.05$), thus confirming that the dynamic increase was most likely present only during the portion of the experiment where the animal was alive.

Additionally, due to the fact that all the in vivo datasets (both gated and ungated) contain data spanning over the 30 minutes, they all comprise a portion of the dynamic activity increase (which is not corrected for). Thus, their mean LV wall activity is always higher than the mean LV wall activity at the beginning of the scan. As a consequence, the microPET LV wall activity needs to be scaled to the activity of one of these reconstructions (and not to the beginning of the scan). This would allow to compare the absolute values of the microPET with those of the in vivo images of interest. A scaling factor was therefore computed by dividing the total LV wall activity of the static reconstruction of the in vivo data by the total LV wall activity of the corresponding microPET reconstruction (statscale). The static reconstruction was chosen as a reference in order not to bias the results towards the dual-gated or partial volume corrected reconstructions—which are the subject of evaluation. The mean statscale factor computed over all sheep was 0.84 ± 0.06.

Data analysis. The max-count polar maps of corresponding ex vivo and in vivo datasets were compared based on their absolute activity differences and on the relative activity distribution.

For the absolute comparison, the scaling factor (as described in the previous section) was applied to the ground-truth datasets prior to any further comparison. Bland-Altman plots were computed between the max-count polar maps of the so-scaled ground-truth and all the in vivo reconstructions, and the bias and limits of agreement were reported. The segments in the Bland-Altman plots were color-coded based on the human vascular regions to which they belong,[19] in order to

verify whether an increased or decreased bias in any of these regions could be observed.

For the relative quantification, Bland-Altman plots were computed between the max-count polar maps of the ground truth and all the in vivo reconstructions, both normalized to their respective maximum value, and the bias and limits of agreement were reported as in.[21] By doing so, we were able to globally highlight whether the differences in the relative myocardial uptake were relevant or negligible. The analysis of the mean bias per segment, over the entire animal cohort, allowed us to pinpoint if and which (set of) segment(s) was particularly responsible for the observed differences.

RESULTS

Absolute Quantification

A plot of the mean activity value in the whole heart, over all animals and for all 10 cardiac gates, was obtained (Figure 2).

We can observe that the downscaled microPET lies in between the curves of the MAP − RR + TV and the OSEM3D + RR. The relative order of the algorithms (OSEM3D + RR is higher than the MAP − RR + TV, which is in turn higher than the uncorrected reconstructions) is similar to what was previously reported in previous studies on partial volume [4] and in agreement with what was expected with motion correction.[22]

In Figures 3 and 4, the Bland-Altman plots for the static reconstructions and for the dual-gated, MAP − RR + TV and OSEM3D + RR reconstructions at two selected cardiac gates (end-systole and end-diastole) are reported. At end-systole, we can appreciate a decrease in bias when the MAP − RR + TV reconstructions are used (− 0.83 vs − 3.74 when static reconstructions are used instead). A slight narrowing of the limits of agreement (4.31 for MAP − RR + TV vs 4.78 for the static reconstructions) can also be observed. Conversely, the OSEM3D + RR reconstructions show a positive bias of 2.99. This is to be expected, since these reconstructions are more noisy and are characterized by overshoots of activity, which produce an overestimation when compared to the microPET. The difference between MAP − RR + TV and OSEM3D + RR is almost as large as the limits of agreement for MAP − RR + TV, thus suggesting that the two methods are in global disagreement[23]—also considering the mean segmental values of the considered datasets, ranging between 8 and 18 SUV.

At end-diastole, a decrease in bias is observed when the OSEM3D + RR reconstructions are considered. Conversely, the bias that is obtained from the MAP − RR + TV reconstructions increases and becomes similar to that of the OSEM3D + RR in absolute values (− 1.90 for MAP − RR + TV vs 1.64 for OSEM3D + RR). This can be explained by the fact that the MAP − RR + TV prior weight is not individually tuned for the various animals, thus possibly leading to greater smoothing in the (differently thinned) walls of the end-diastolic phase.

The MAP − RR + TV image is however superior in terms of noise properties when compared to the corresponding OSEM3D + RR reconstructions, as Figure 5 illustrates.

Relative Quantification

The Bland-Altman plots obtained from the normalized max-count polar maps of the dual-gated MAP − RR + TV, OSEM3D + RR (end-systole), and the static reconstructions reveal very small differences compared to the ground truth (graphs not shown). The biases for all reconstruction and motion correction methods are below the 0.03 level, indicating an overall difference of less than 3% between the normalized polar maps of the in vivo datasets and the ground truth. The analysis of the bias *per segment* revealed a particularly negative bias for the segment 3 and 9 (− 0.22 and − 0.13, respectively) and a positive bias for segment 11 (+ 0.12), when the static reconstructions are considered. As for the dual-gated reconstructions, a particular bias is observed for segments 3 (− 0.15 for MAP − RR + TV and − 0.12 for OSEM3D + RR) and 17 (+ 0.12 for MAP − RR + TV and + 0.11 for OSEM3D + RR). Figure 6 visually reports on the mean bias and standard deviation per segment, over the entire animal cohort, and allows us to visualize the aforementioned segments—i.e., those most responsible of the observed differences.

DISCUSSION

PET is an important tool to assess myocardial perfusion and flow reserve, myocardial viability, and has a great potential in emerging clinical applications such as quantification of tracer uptake in atherosclerotic plaques. Since PET images provide a multitude of information, quantitative measurements are important, and allow to reduce observer variability. Therefore, the goal of this study was to optimize absolute quantification of myocardial tracer uptake compared to standard clinical reconstructions. We used 18F-FDG, a widely available tracer with relatively long half-life (109 min), which allowed us to perform both in vivo imaging and afterwards *ex vivo* imaging serving as reference unaffected by cardiac or respiratory motion. This would not have been possible with short-lived tracers (e.g., 11C-tracers or available perfusion tracers). The use of 18F-FDG is further supported by studies showing that FDG

uptake is correlated with pressure-strain loop areas in patients with left bundle branch block, hence serving as a non-invasive measurement of myocardial work.[2] Another study comparing FDG and 18F-FTHA (fatty acid tracer) in patients with congestive heart failure demonstrated a shift in substrate metabolism which may be an indicator of impaired energy efficiency during heart failure.[24]

This study correlates the tracer uptake in motion-corrected and static cardiac datasets to the tracer uptake of a scaled ex vivo ground truth, as a first attempt to pinpoint the optimal reconstruction method for absolute and relative quantification of cardiac datasets. Both cardiac and respiratory motions were corrected for in the considered in vivo datasets. In fact, it has been previously demonstrated that the combination of cardiac and respiratory motion correction leads to a more accurate estimation of myocardial uptake and a significant effect on resolution, and state-of-the-art motion correction methods nowadays aim at correction of both motions.[25-28]

In this work, we assumed that the intravascular activity in the myocardial wall is small compared to the trapped FDG and can be ignored with good approximation, because the in vivo images are acquired between 30 and 60 minutes after the injection.

The Bland-Altman plots report an improvement when motion correction is applied to the considered datasets. Additionally, the graph showing the mean activity computed on the max-count polar maps of the in vivo reconstructions shows a ranking that is similar to what was observed in a previous study on ex vivo datasets, where the OSEM3D + RR over-estimated the total activity and the MAP − RR + TV was the closest to the ground truth.[4] This gives a first indication that the results previously obtained on ex vivo datasets can be transferred to the in vivo scenario.

The similarity to the ground truth is maximal for the end-systolic gate, which is the gate characterized by thicker walls and thus less prone to blurring due to PVE or to the suboptimal choice of the MAP − RR + TV weight and smoothing mask. A smaller bias was expected when the MAP − RR + TV prior and the end-diastolic gate were considered. In this latter case, a similar bias (absolute value) is observed for the MAP − RR + TV and the OSEM3D + RR reconstruction, thus questioning the necessity of the additional application of prior information. However, a more tailored tuning of the TV prior parameters to the specific subject may reduce this bias. MAP − RR + TV images are anyway less noisy, and at worst as far from the ground truth as the OSEM3D + RR (in absolute value), for what absolute quantification is concerned.

A number of limitations are connected to the current experimental setup, which used the microPET datasets as ground truth for PVC and motion correction techniques.

In our previous work[4] we compared the images of the ex vivo hearts obtained from the microPET and the Hirez scanner, and their differences and similarities were extensively described. In that study, we concluded that the ex vivo reconstructions with the non-anatomical prior achieved very good similarity to the microPET images, hence we can exclude that the differences between ex vivo and in vivo datasets are due to differences in reconstruction algorithm and partial volume effects. Two remaining factors, i.e., attenuation correction and scatter correction, could however still have a contribution to the in vivo datasets. This is a limitation of the current experimental setup. An in vivo scan of the intact sheep after stopping the heart could have excluded the interference of the motion and have an intermediate in vivo image to use as a reference. However this was impossible due to governing standard operating procedures that do not allow to sacrifice animals in the scanner room and animals had to be moved to a dedicated room at distance for sacrifice. Hence, no scans could be performed during the time between the end of the in vivo scans and the sacrifice of the animal, and the microPET datasets were scanned about an hour after the end of the in vivo scans. During this time, the activity concentration kept on increasing. The reconstruction of the dynamic frames of the acquired in vivo datasets helped to estimate a trend of FDG uptake for the LV myocardium over time. The obtained curves, for each of the analyzed animals, corroborated those of a previous study which observed increased FDG uptake up to 3 hours after tracer injection.[18]

Therefore, a method to correlate the microPET and the in vivo absolute values was also proposed in this work, which downscaled the total activity of the LV wall of the microPET reconstructions to match the total reconstructed LV wall activity of the in vivo datasets. This was necessary to take into account the dynamic increase of the FDG uptake with time. The microPET was scaled using the total activity of the static reconstructions, in order not to bias the conclusions towards one of the algorithms we wanted to evaluate. Despite all efforts to calculate the scaling factor in a sensible way, we cannot exclude that the use of a scaling factor might have biased all results towards one or the other reconstruction algorithm. However, the ranking of the algorithms reflected what was reported in previous literature. Additionally, the absolute activity values obtained at end-systole confirm that the proposed scaling technique can represent a reasonable trade-off. Although

this is a limitation of the current experimental setup, we believe that this is an accurate scale factor estimation, additionally confirmed by the fact that the scaled microPET LV wall activity is similar to the estimated LV wall activity at sacrifice time.

We additionally correlated the relative distribution of activity within the LV wall of the in vivo and the ex vivo datasets, to assess whether the regional activity distribution would be affected by the different motion correction techniques. We observed that neither reconstruction method affected the activity distribution within the in vivo sheep hearts, nor improved the similarity to the ground truth. This can be explained by the fact that, in the analyzed sheep, a similar blurring affected both the septum and the lateral wall due to respiration, and the differences in wall thickness were not so pronounced to determine a stronger blurring on one or the other side of the LV wall due to the partial volume effect. The analysis of the Bland-Altman plots on the normalized polar maps confirmed such visual observation and an overall good similarity of the normalized in vivo polar maps to the ground truth. Some segments, in the inferoseptal and inferolateral portion of the LV wall, revealed bigger discrepancies in the activity distribution, when the in vivo and the ex vivo scans are compared. This may be caused by the different shapes and sizes of the ex vivo and the in vivo datasets, which could affect the perfect alignment of corresponding structures. Additionally, the filling of the ex vivo hearts with the polyurethane foam might have stretched and possibly modified the relative activity distribution in some of the datasets. Another possible explanation of this change in activity distribution is that the sacrifice of the sheep using KCl caused a sudden and unexpected shift of tracer uptake in the heart. However, none of these hypotheses could be verified with the available sheep datasets.

A question still left open is the transferability of these results to human studies. Further experiments would be needed to clarify whether the use of motion correction is as irrelevant as in this sheep study for relative LV wall quantification. A comparison of the non-corrected vs the motion-corrected reconstructions of animal and human datasets would be valuable to clarify this point. However, at present, all available human datasets showed a very irregular breathing pattern (acquired via a respiratory tracking system), with baseline drifts and sudden amplitude changes which made it impossible to perform accurate motion correction, without having to exclude a significant amount of the data. In addition to baseline drifts and unavoidable signal losses due to the nature of the breathing patterns of the patients, these external tracking devices also record the external motion of the abdomen, which needs to be translated into a corresponding internal motion of the heart. Improved motion correction techniques should be implemented in the first place, to allow an event-by-event motion correction such that the motion-corrected vs the static reconstructions could be analyzed (e.g., as in[29]). This, combined with cardiac motion compensation, and achieved within times that are compatible with clinical practice, could produce images with excellent noise properties. However, the heart motion is very non-rigid, and exact compensation for this motion is difficult. Proposed promising solutions to address this include the use of a cardiac deformation field from MR to reconstruct a single image from all gates.[30,31] In the absence of accurate motion estimation, the risk of producing an inaccurate representation of the heart is not negligible. In these cases, a great improvement could be already achieved if only respiratory motion compensation and a frame-by-frame reconstruction for the cardiac motion was performed, especially when in combination with non-anatomical priors. Seeing the beating heart could still be useful and have clinical value during the diagnosis, and we would expect that the end-systolic image (using all respiratory gates) would still be much better than a single double-gated frame improperly corrected for. The additional combination of motion compensation with resolution modeling and non-anatomical priors would further improve cardiac wall homogeneities and quantitative accuracy.

NEW KNOWLEDGE GAINED

This work addresses the previously unanswered question regarding the usefulness of non-anatomical priors in combination with motion correction for the quantification of cardiac PET images. The study design compares in vivo cardiac datasets acquired on a clinical scanner to datasets on a pre-clinical small animal and therefore high-resolution scanner is innovative and original.

CONCLUSION

We have explored the feasibility of an ex-to-in vivo comparison for the purpose of evaluating the benefits of combined motion and partial volume correction. The available data suggest that the use of motion- and partial volume correction techniques (e.g., MAP reconstruction with a well-tuned edge-preserving prior, such as TV) does not hamper relative quantification and enhances the noise properties of the resulting images of the heart. It is advisable to use the end-systolic gate when quantification of cardiac datasets is aimed at, such that absolute quantification is improved.

Acknowledgements

The authors wish to thank Charles Watson and Judd Jones for their help with the Siemens data processing.

Author Contributions

AT was responsible for the study design, the simulation setup, the reconstructions, and the data collection and analysis, and drafted the manuscript. JD was also responsible for the data collection. JN and KV assisted with the study design, the analysis of data, and the careful revision of the manuscript. JUV, FR, PC, JD, and OG participated in the study design and critically revised the manuscript. All authors read and approved the final manuscript.

Disclosure

The authors declare that they have no competing interests.

References

1. Schindler TH. Cardiac PET/computed tomography applications and cardiovascular outcome. PET Clin 2015;10:441-59.
2. Russell K, Eriksen M, Aaberge L, Wilhelmsen N, Skulstad H, Remme EW, et al. A novel clinical method for quantification of regional left ventricular pressure-strain loop area: A non-invasive index of myocardial work. Eur Heart J 2012;33:724-33.
3. Nowak B, Sinha AM, Schaefer WM, Koch KC, Kaiser HJ, Hanrath P, et al. Cardiac resynchronization therapy homogenizes myocardial glucose metabolism and perfusion in dilated cardiomyopathy and left bundle branch block. J Am Coll Cardiol 2003;41:1523-8.
4. Turco A, Nuyts J, Duchenne J, Gheysens O, Voigt J-U, Claus P, et al. Analysis of partial volume correction on quantification and regional heterogeneity in cardiac PET. J Nucl Cardiol 2017. https://doi.org/10.1007/s12350-016-0773-z.
5. Chambolle A, Pock T. A first-order primal-dual algorithm for convex problems with applications to imaging. J Math Imaging Vis 2011;40:120-45.
6. Ter-Pogossian MM, Bergmann SR, Sobel BE. Influence of cardiac and respiratory motion on tomographic reconstructions of the heart: Implications for quantitative nuclear cardiology. J Comput Assist Tomogr 1982;6:1148-55.
7. Ahmed MA, Xiao P, Xie Q. New approach for simultaneous respiratory and cardiac motion correction in cardiac PET (NAMC-CPET). Phys Med Biol. 2015;60:7779.
8. Buther F, Dawood M, Stegger L, Wubbeling F, Schafers M, Schober O, et al. List mode-driven cardiac and respiratory gating in PET. J Nucl Med 2009;50:674-81.
9. Kokki T, Sipilä HT, Teräs M, Noponen T, Durand-Schaefer N, Klén R, et al. Dual gated PET/CT imaging of small targets of the heart: Method description and testing with a dynamic heart phantom. J Nucl Cardiol 2010;17:71-84.
10. Duchenne J, Claus P, Turco A, Vunckx K, Pagourelias E, Haemers P, et al. A new animal model of rapid pacing-induced dilated cardiomyopathy and LBBB. Eur Heart J 2015;16:P145.
11. Kim J (2009) Hyperinsulinemic euglycemic clamp to assess insulin sensitivity in vivo. In: C. Stocker (ed.) Type 2 diabetes, Methods in Molecular Biology, vol. 560. Humana Press, New York. ISBN 978-1-934115-15-2
12. Dawood M, Büther F, Lang N, Schober O, Schäfers KP. Respiratory gating in positron emission tomography: A quantitative comparison of different gating schemes. Med Phys 2007;34:3067-76.
13. Alessio AM, Rahmim A, Orton CG. Resolution modeling enhances PET imaging. Med Phys 40:120601. https://doi.org/10.1118/1.4894496
14. Vunckx K, Atre A, Baete K, Reilhac A, Deroose CM, Van Laere K, Nuyts J. Evaluation of three MRI-based anatomical priors for quantitative PET brain imaging. IEEE Trans Med Imaging 2012;31:599-612.
15. Turco A, Nuyts J, Gheysens O, Duchenne J, Voigt J-U, Claus P, Vunckx K. Lesion quantification and detection in myocardial 18F-FDG PET using edge-preserving priors and anatomical information from CT and MRI: A simulation study. EJNMMI Phys 2016;3:1-32.
16. De Man B, Basu S. Distance-driven projection and backprojection in three dimensions. Phys Med Biol 2004;49:2463.
17. Brambilla M, Secco C, Dominietto M, Matheoud R, Sacchetti G, Inglese E. Performance characteristics obtained for a new 3-dimensional lutetium oxyorthosilicate based whole-body PET/CT scanner with the National Electrical Manufacturers Association NU 2-2001 Standard. J Nucl Med 2005;46:2083-91.
18. Cheng G, Alavi A, Lim E, Werner TJ, Del Bello CV, Akers SR. Dynamic changes of FDG uptake and clearance in normal tissues. Mol Imaging Biol 2013;15:345-52.
19. Cerqueira MD, Weissman NJ, Dilsizian V, Jacobs AK, Kaul S, Laskey WK, et al. Standardized myocardial segmentation and nomenclature for tomographic imaging of the heart a statement for healthcare professionals from the cardiac imaging committee of the Council on Clinical Cardiology of the American Heart Association. Circulation 2002;105:539-42.
20. Nuyts J, Mortelmans L, Suetens P, Oosterlinck A, de Rou M. Model-based quantification of myocardial perfusion images from SPECT. J Nucl Med 1989;30:1992.
21. Altman DG, Bland JM. Measurement in medicine: The analysis of method comparison studies. Statistician 1983;32:307-17.
22. Rubeaux M, Doris MK, Alessio A, Slomka PJ. Enhancing cardiac PET by motion correction techniques. Curr Cardiol Rep. 2017;19:14.
23. Giavarina D. Understanding Bland Altman analysis. Biochem Med. 2015;25:141-51.
24. Taylor M, Wallhaus TR, DeGrado TR, Russell DC, Stanko P, Nickles RJ, et al. An evaluation of myocardial fatty acid and glucose uptake using PET with [18F] fluoro-6-thia-heptadecanoic acid and [18F] FDG in patients with congestive heart failure. J Nucl Med 2001;42:55-62.
25. Lamare F, Le Maitre A, Dawood M, Schäfers K, Fernandez P, Rimoldi O. Evaluation of respiratory and cardiac motion correction schemes in dual gated PET/CT cardiac imaging. Med Phys 2017;41:72504.
26. Martinez-Möller A, Zikic D, Botnar RM, Bundschuh RA, Howe W, Ziegler SI, et al. Dual cardiac-respiratory gated PET: Implementation and results from a feasibility study. Eur J Nucl Med Mol Imaging 2007;34:1447-54.
27. Büther F, Dawood M, Stegger L, Wübbeling F, Schäfers M, Schober O, et al. List mode-driven cardiac and respiratory gating in PET. J Nucl Med 2009;50:674-81.
28. Gigengack F, Ruthotto L, Burger M, Wolters CH, Jiang X, Schafers KP. Motion correction in dual gated cardiac PET using mass-preserving image registration. IEEE Trans Med Imaging 2012;31:698-712.

29. Cal-Gonzalez J, Lassen M, Rasul S, Beitzke D, Schaefers K, Hacker M, et al. Joint respiratory and cardiac motion compensation: Application to cardiac PET/CT and PET/MR imaging. Paper presented at the international conference on nuclear cardiology and cardiac CT (ICNC, Vienna), 2017.
30. Rahmim A, Tang J, Zaidi H. Four-dimensional image reconstruction strategies in cardiac-gated and respiratory-gated PET imaging. PET Clin 2013;8:51-67.
31. Küstner T, Schwartz M, Martirosian P, Gatidis S, Seith F, Gilliam C, et al. MR-based respiratory and cardiac motion correction for PET imaging. Med Image Anal 2017;42:129-44.